

Research Article

Lift Augmentation on a Tiltrotor Wing Using the Combination of Vortex Generators and Gurney's Flap

Hao Chen , Siliang Du , and Zhong Chen 

Jiangsu Key Laboratory of Advanced Manufacturing Technology, Huaiyin Institute of Technology, 223003 Huaian, Jiangsu, China

Correspondence should be addressed to Hao Chen; chenhao@hyit.edu.cn and Siliang Du; kjofchina@qq.com

Received 18 June 2023; Revised 11 August 2023; Accepted 25 August 2023; Published 7 September 2023

Academic Editor: Vijayanandh Raja

Copyright © 2023 Hao Chen et al. This is an open access article distributed under the Creative Commons Attribution License, which permits unrestricted use, distribution, and reproduction in any medium, provided the original work is properly cited.

Recently, flow control using vortex generators (VGs) and a Gurney flap (GF) has received considerable attention, but independently. The purpose of this study is to perform a numerical investigation into the lift augmentation effects of a tiltrotor wing with the combination of VGs and GF. The numerical results were obtained with the Reynolds-averaged Navier-Stokes (RANS) equations, and the turbulence was solved by the Spalart-Allmaras one-equation turbulence model. The separate and joint performances of these two control devices at different angles of attack are determined. It is shown that the combined configuration can provide greater lift augmentation than either device individually. Compared with the baseline wing, the implementation of both devices increases the stall angle of attack from 10° to 22° , and the maximum lift coefficient is improved by 82.33%.

1. Introduction

Tiltrotor aircraft is a unique type of flying vehicle that combines the vertical takeoff and landing capability of a helicopter with the high-speed cruise performance of a turboprop aircraft. Due to structural design considerations, the wings are of small span, and they must be thick enough to accommodate the rotor shaft for power transmission. However, the comparatively high thickness makes tiltrotor aircraft particularly susceptible to stall [1]. On the other hand, during the course of conversion, the rotors which produce the lift gradually transition to provide aircraft thrust. If the wing-generated lift is not sufficient to against gravity, the aircraft may encounter serious flight accidents. Consequently, boundary layer control is critical, and the design of lift-enhancing devices is an important problem for tiltrotor aircraft.

In recent years, various flow control techniques have been developed for aerodynamic improvements. In general, these techniques can be divided into passive and active control methods depending on whether external energy is required [2]. Compared with active control technology, passive control offers a simple structure and is inexpensive. Vortex generators (VGs) are among the most effective passive control devices.

First documented by Taylor [3], the VGs are composed of a row of small plates that are mounted normal to the wing surface. The streamwise vortices induced by VGs can enhance the momentum mixing and thus reduce or eliminate boundary layer separation. Numerous numerical simulations [4, 5] and experimental tests [6, 7] have been carried out to determine the influence of VGs. A detailed, comprehensive review was presented by Zhao et al. [8]. Several studies [9, 10] mentioned that the counterrotating VGs have a higher tendency to delay flow separation, as compared to corotating configuration. Additionally, triangular shape VGs were better performing than rectangular shape VGs in terms of lift augmentation and drag reduction, as reported by Fouatih et al. [11]. The presence of VGs at the quarter-chord location along the XV-15 wing eliminated the premature stall [12]. A similar result was noticed when VGs were added to the midwing fairing of the V-22 aircraft [13].

On the other hand, the Gurney flap (GF) is also a simple high-lift device consisting of a short flat plate placed over the pressure side of the airfoil. In 1978, Liebeck [14] conducted the first wind-tunnel experiment with GFs. The results showed that GF works by increasing the effective camber of the airfoil. Inspired by this, GFs have been extensively



FIGURE 1: Schematic diagram of the A821201 wing equipped with VGs and GF.

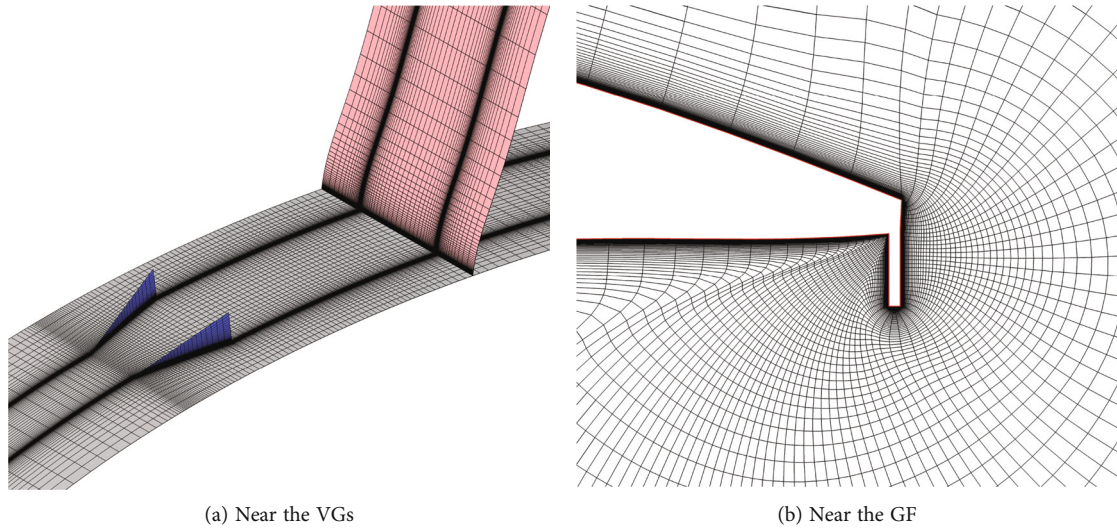


FIGURE 2: Computational grid of the controlled A821201 wing.

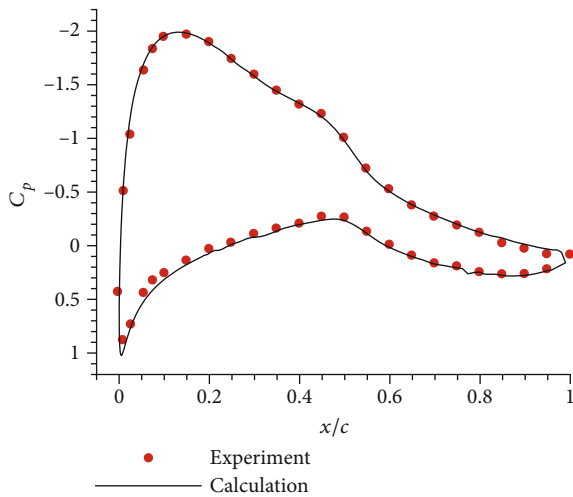


FIGURE 3: Comparison of pressure distributions of an A821201 infinite straight wing.

investigated and applied to a wide range of fields, such as static and dynamic stall control [15, 16], shock wave control [17, 18], and rotor blade load control [19, 20]. The work by Wang et al. [21] provides a comprehensive review of its applications. In recently years, in-depth studies have been carried out to explore the effects of geometrical parameters, including height, chordwise location, and mounting angle. Li et al. [22] and Date and Turnock [23] performed experimental investigations and computational simulations on a NACA 0012 profile with GFs. The results revealed that GF height is a significant factor. The impacts of chordwise position were assessed by Baker et al. [24], and they suggested that GFs are most effective when located at the trailing edge. Moreover, the best aerodynamic performance was achieved with the mounting angle of 90° [25].

As indicated by the aforementioned literature survey, there has been a great deal of researches on the effect of VGs or GF. However, the simultaneous application of VGs and GF is seldom studied, and the combined effects remain

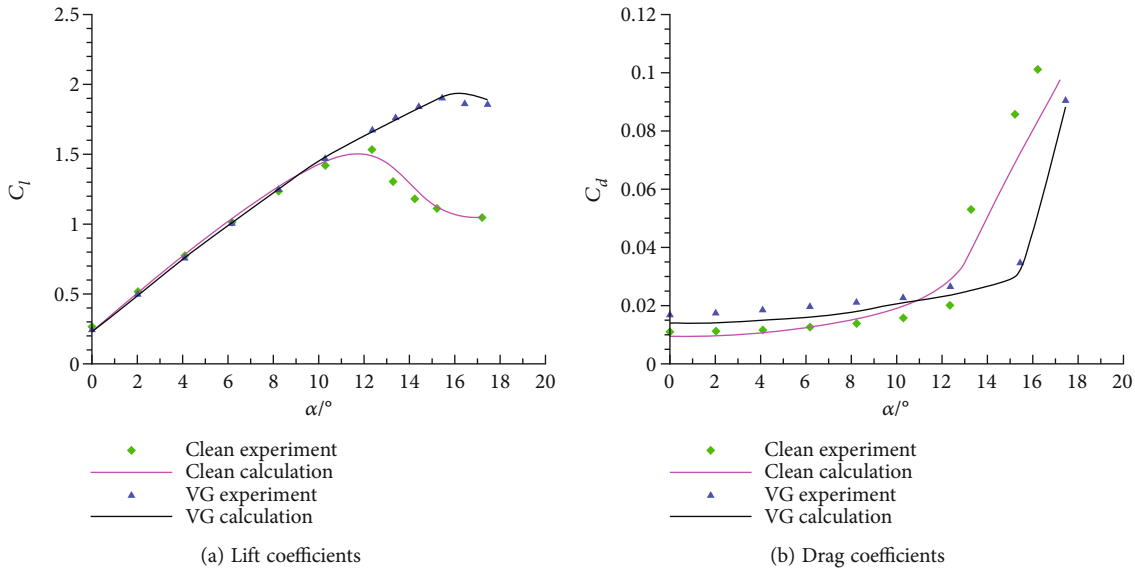


FIGURE 4: Comparison of aerodynamic coefficients of a DU97-W-300 airfoil without and with VGs.

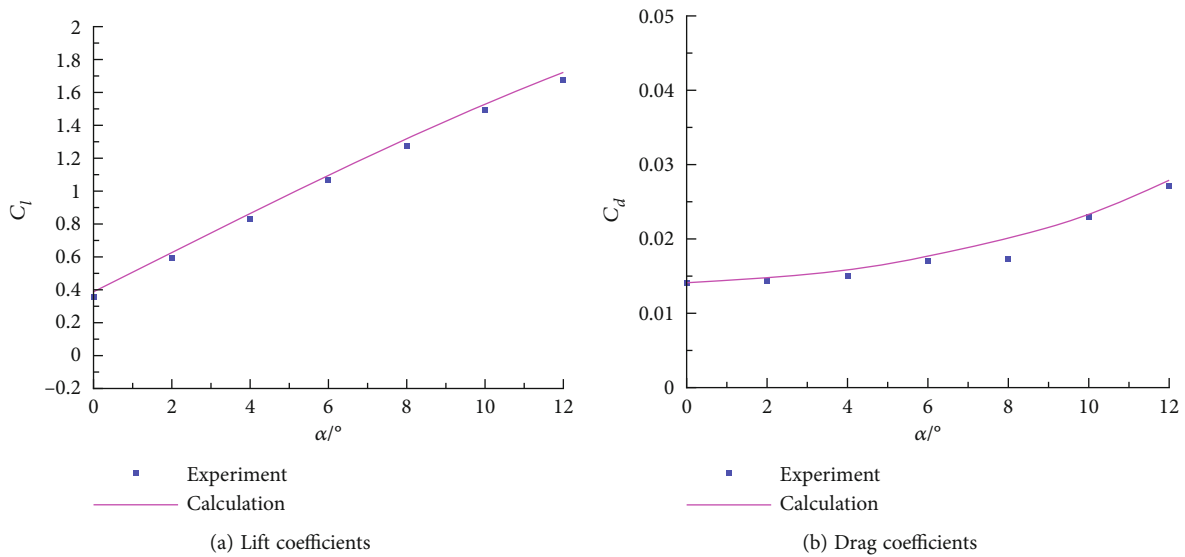


FIGURE 5: Comparison of aerodynamic coefficients of a NACA 0012 airfoil with a 2% chord GF.

unclear. The present work thereby is aimed at investigating the joint performances of these two devices for a tiltrotor wing. The structure of this paper is as follows. The geometrical model and grid generation are given in Section 2. Section 3 presents a description of the numerical approach. The results are discussed in Section 4, and conclusions follow in Section 5.

2. Geometry Modeling and Grid Generation

The chosen profile was generated by Bell Helicopter particularly for use on the V-22 tiltrotor wing and is designated as A821201 airfoil [26]. Figure 1 depicts a schematic diagram of the design geometry. As can be seen, VGs are installed on the upper surface, and the VG arrangement is depended

on five variables: height h_{VG} , length L , spanwise spacing d , orientation angle β , and chordwise positioning x_{VG} . In addition, h_{GF} represents the height of GF. In the present simulations, the chord length of wing is 650 mm, the span length is 35 mm, and the value of spacing d is 17.5 mm [7]. The VGs are set as zero-thickness surfaces, and the thickness of GF is 1 mm.

In order to reduce the computational burden, only one pair of VGs is simulated with the periodic condition imposed on spanwise boundaries [27]. The O-H type structured grid is used with a normal grid spacing of 1×10^{-6} chords at the wall surface, and the farfield boundary is located at 30 chords. Figure 2 shows the close-up view of computational grid. Grid clustering is evident near the surface of VGs, as well as the trailing edge.

3. Numerical Methodology

3.1. *Governing Equations.* Based on the Cartesian coordinates, the three-dimensional unsteady Navier-Stokes equations can be formulated as [28]

$$\frac{\partial \mathbf{W}}{\partial t} + \frac{\partial \mathbf{F}}{\partial x} + \frac{\partial \mathbf{G}}{\partial y} + \frac{\partial \mathbf{Q}}{\partial z} = \frac{\partial \mathbf{R}}{\partial x} + \frac{\partial \mathbf{S}}{\partial y} + \frac{\partial \mathbf{T}}{\partial z}, \quad (1)$$

where \mathbf{W} is the state vector and written as

$$\mathbf{W} = \begin{bmatrix} \rho \\ \rho u \\ \rho v \\ \rho w \\ \rho E \end{bmatrix}. \quad (2)$$

\mathbf{F} , \mathbf{G} , and \mathbf{Q} represent the convective flux vectors and expressed as

$$\mathbf{F} = \begin{bmatrix} \rho u \\ \rho u^2 + p \\ \rho uv \\ \rho uw \\ \rho uE + up \end{bmatrix}, \quad \mathbf{G} = \begin{bmatrix} \rho v \\ \rho vu \\ \rho v^2 + p \\ \rho vw \\ \rho vE + vp \end{bmatrix}, \quad (3)$$

$$\mathbf{Q} = \begin{bmatrix} \rho w \\ \rho wu \\ \rho wv \\ \rho w^2 + p \\ \rho wE + wp \end{bmatrix}.$$

In the above expressions, u , v , and w are the Cartesian velocity components, ρ denotes the density, and E stands for the total energy per unit mass. \mathbf{R} , \mathbf{S} , and \mathbf{T} are the viscous flux vectors. Pressure p is calculated as

$$p = (\gamma - 1)\rho \left[E - \frac{1}{2}(u^2 + v^2 + w^2) \right], \quad (4)$$

where γ is the specific heat ratio with the value of 1.4 for ideal gas.

The finite volume method is adopted for spatial discretization with a second-order accuracy central difference

TABLE 1: The main parameters of calculated configurations.

Configuration	Vortex generators				Gurney flap
	x_{VG}/c	h_{VG} (mm)	L (mm)	β ($^\circ$)	h_{GF} (mm)
Baseline	—	—	—	—	—
VG1	0.2	2.5	15	15	—
VG2	0.2	5	15	15	—
VG3	0.2	5	25	15	—
VG4	0.2	5	15	10	—
VG5	0.2	5	15	20	—
VG6	0.1	5	15	15	—
VG7	0.4	5	15	15	—
GF1	—	—	—	—	3.25
GF2	—	—	—	—	6.5
GF3	—	—	—	—	13
VG6+GF2	0.1	5	15	15	6.5

TABLE 2: Grid independency study of the A821201 wing using the combination of VG6 and GF2 at $\alpha = 10^\circ$.

Mesh	C_l	C_d	C_l/C_d
Coarse	1.9179	0.0334	57.4222
Medium	1.9286	0.0330	58.4424
Fine	1.9311	0.0329	58.6960

scheme, and the dual time-stepping algorithm with subiterations is utilized for time discretization. All simulations presented herein use the Spalart-Allmaras one-equation turbulence model, which can provide excellent predictions of flows involving the implementation of flow control technologies [29]. At the farfield boundary, the characteristic boundary condition with the Riemann invariants is employed and the no-slip boundary condition is applied on the wall surface. This flow solver is developed by our research group and has been frequently applied to the aerodynamic calculations.

3.2. *Validation.* Three different cases were considered for code validation. The first case is an A821201 infinite straight wing. In this case, the Mach number is 0.13, and the angle of attack is 7° . As depicted in Figure 3, the computed pressure distributions are in good accordance with the experimental values [30].

Because of lacking the experimental data of the A821201 airfoil equipped with VGs, present numerical modeling is validated against the experimental data of the DU97-W-300 profile. The Mach number is 0.13 with a Reynolds number of 2.0×10^6 , and the VG geometric parameters can be found in Ref. [7]. As seen in Figure 4, the calculated aerodynamic coefficients show good agreement with the measurements.

The following case is a NACA 0012 airfoil fitted with a 2% chord GF. The wind-tunnel test was conducted at a Mach number of 0.088, yielding a Reynolds number of 2.1×10^6 . The results were compared with the experimental data of Li et al. [22]. As shown in Figure 5, very good

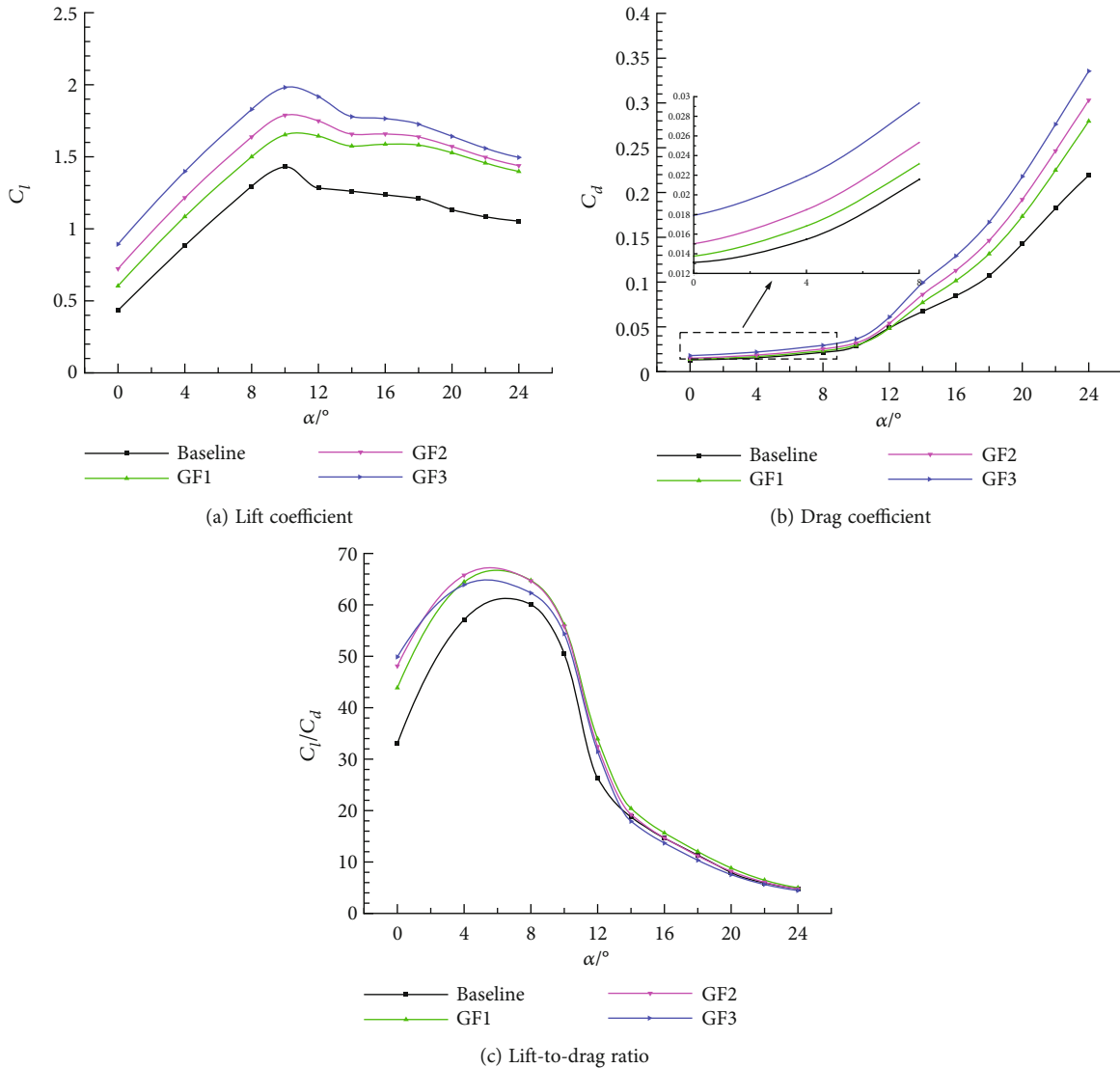


FIGURE 6: Comparison of aerodynamic coefficients without and with different GFs.

agreement was also found between numerical predictions and experimental results, thus demonstrating the accuracy and reliability of the present flow solver.

4. Results and Discussion

In this section, all simulations are undertaken at a Mach number of 0.3, which corresponds to a chord Reynolds number of 4.54×10^6 . Table 1 summarizes the calculated configurations, and the symbol “-” represents “without.” In our previous works [31, 32], seven VG arrangements (VG1 to VG7) were studied, and the impact of different parameters has been discussed qualitatively and quantitatively. To avoid redundant publication, it is not described here. By comparison, VG6 shows the best aerodynamic performance among those configurations. In the current work, the effects of GF size on lift enhancement are firstly determined. The GF heights are 3.25 mm (GF1), 6.5 mm (GF2), and 13 mm (GF3), respectively, and the corresponding nondimensional

heights are 0.5%, 1%, and 2% of the wing chord. Then, VG6 and GF2 are simultaneously applied to the baseline wing to evaluate the combined effects.

4.1. Grid Independence Study. To examine the grid sensitivity, three different grids were computed: 2,453,139 (coarse), 4,249,077 (medium), and 6,272,545 (fine). Table 2 indicates that the differences between medium and fine grids are negligible. Thus, the medium grid was used throughout this study.

4.2. Effect of the Gurney Flap. Figure 6 shows the calculation results of the A821201 wing without and with different GFs. As seen in Figure 6(a), the addition of GF produces a significant lift increment compared with the baseline wing. Simultaneously, the larger the GF height, the more the lift augments. The maximum lift coefficient is increased by 15.59%, 25.06%, and 38.55% for GF1, GF2, and GF3, respectively. The results also suggest that the stall angle is unaltered

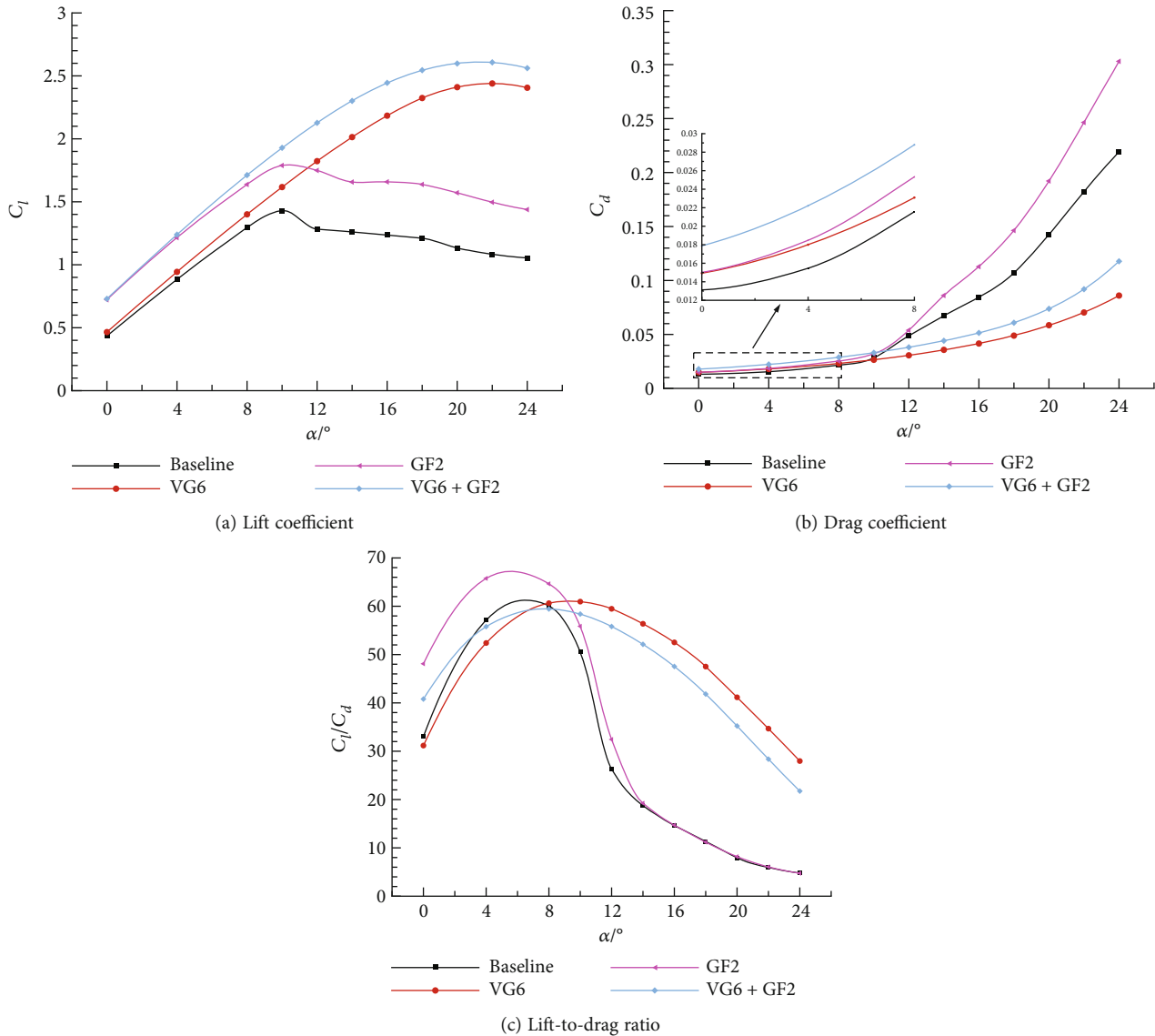


FIGURE 7: Comparison of aerodynamic coefficients for the uncontrolled and controlled cases.

under the control of GF, which draws the same conclusion as in Ref. [33]. As illustrated in Figure 6(b), substantial drag increment is found when GF height is increased to 2% chord. Figure 6(c) presents the characteristics of lift-to-drag ratio. Increments in the lift-to-drag ratio are evident when $\alpha < 12^\circ$. At $\alpha = 4^\circ$, the installation of GF2 is an optimal design, and in this case, the lift-to-drag ratio is increased by 15.12% compared with that of baseline wing.

4.3. Effect of Joint Vortex Generators and Gurney's Flap. As previously mentioned, VGs can delay boundary layer separation but the enhancement of lift coefficient at small angles of attack is not evident, whereas the GF shows the opposite characteristics. By combining the advantages of these two devices, in this work, an extended numerical analysis is carried out using the synergism of VG6 and GF2. Figure 7 shows the aerodynamic coefficients for four scenarios such as baseline, baseline with VG6, baseline with GF2, and base-

line with both VG6 and GF2. As seen in Figure 7(a), the overall lift characteristics are greatly enhanced with the combination of VG6 and GF2. The reason is that the wing camber is increased by the GF, while the flow separation at high angles of attack is suppressed by the VGs. In comparison with the clean wing, the combined configuration increases the maximum lift coefficient by 82.33%. However, as shown in Figure 7(b), the implementation of both devices is accompanied by a certain drag penalty at small angles of attack. Figure 7(c) presents the characteristics of lift-to-drag ratio. It shows that the combined drag penalty leads to reduced lift-to-drag ratio with respect to the baseline in the range of 4° to 8° .

For better understanding, the streamlines at the middle plane around different configurations are presented in Figure 8. In the case of baseline, as well as GF2, when $\alpha = 10^\circ$, there exists a small separation bubble over the suction surface; when $\alpha = 20^\circ$, the flow is mostly separated. For the

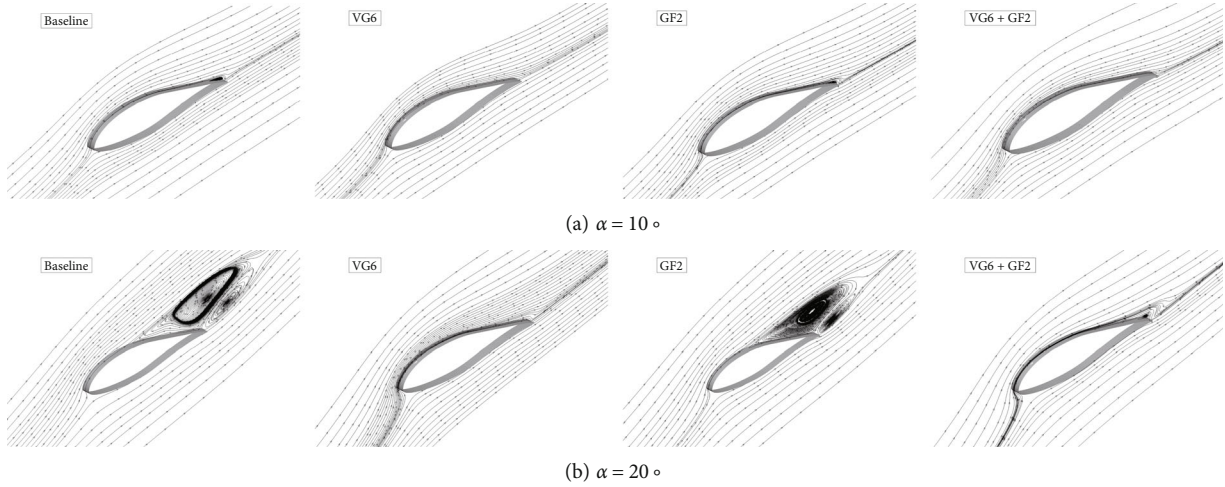


FIGURE 8: Comparison of streamlines for the uncontrolled and controlled cases.

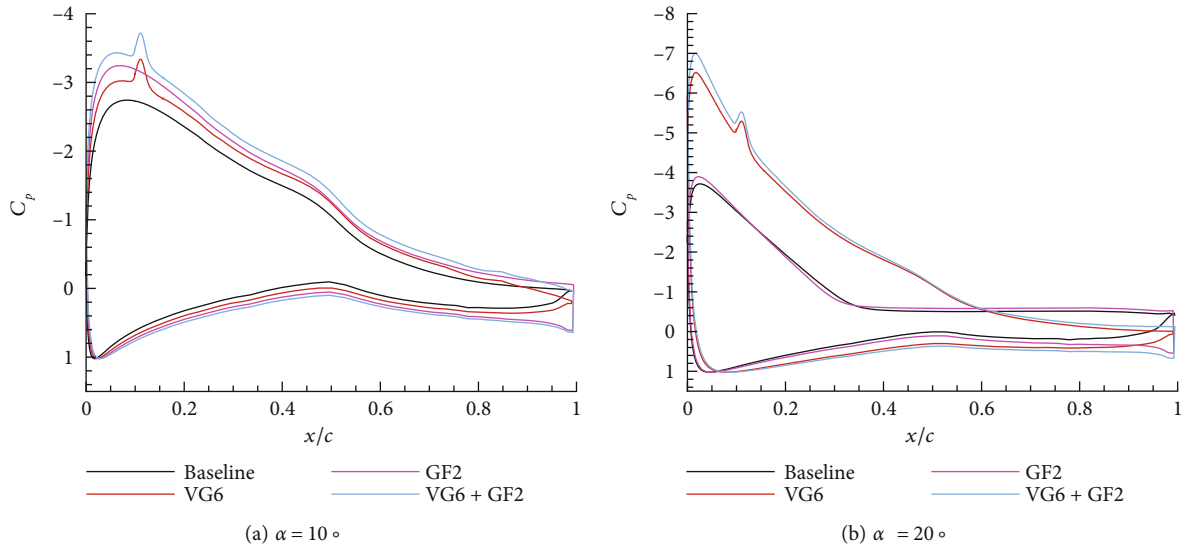


FIGURE 9: Comparison of pressure distributions for the uncontrolled and controlled cases.

TABLE 3: Comparison of aerodynamic performance parameters for the uncontrolled and controlled cases.

Configuration	$C_{l\alpha}$	$C_{l,max}$	α_{stall}
Baseline	6.18 rad ⁻¹	1.43	10°
VG6	6.70 rad ⁻¹	2.44	22°
GF2	6.58 rad ⁻¹	1.79	10°
VG6+GF2	7.04 rad ⁻¹	2.61	22°

single application of VG6, there is no obvious flow separation at the same angles of attack. With the combination of VG6 and GF2, although a recirculation region occurs at $\alpha = 20^\circ$, the scale of the separation region is largely reduced. Figure 9 illustrates the comparison of pressure coefficients for the uncontrolled and controlled cases. The pressure distributions are extracted along the wing centerline. It is apparent that the suction peak over the upper surface is further improved by the combined configuration. The detail data of the lift-curve slope ($C_{l\alpha}$), the

maximum lift coefficient ($C_{l,max}$), and the stall angle of attack (α_{stall}) are listed in Table 3. It is shown that the combination of VG6 and GF2 can result in remarkable enhancements of lift characteristics.

5. Conclusions

In this paper, the influence of vortex generators, Gurney’s flap, and their combination on the aerodynamic performance of an A821201 wing is numerically investigated. Based on the present results, the conclusions are as follows:

- (1) The vortex generators can effectively suppress the flow separation and augment the lift coefficient at high angles of attack
- (2) The Gurney flap can increase the effective camber of the airfoil and has the ability to improve the lift coefficient significantly at small angles of attack.

However, the stall angle remains unchanged compared to the baseline wing

- (3) The vortex generators and Gurney flap can work in concert to provide better lift characteristics than either device alone. The overall aerodynamic performance is greatly enhanced with the combination of these two control devices

Nomenclature

Latin Symbols

c :	Airfoil chord length
C_d :	Drag coefficient
C_l/C_d :	Lift-to-drag ratio
C_l :	Lift coefficient
$C_{l,max}$:	Maximum lift coefficient
$C_{l\alpha}$:	Lift-curve slope
C_p :	Pressure coefficient
d :	Spanwise spacing of vortex generator
E :	Total energy per unit mass
F, G, Q :	Convective fluxes
h_{GF} :	Height of the Gurney flap
h_{VG} :	Height of vortex generator
L :	Length of vortex generator
p :	Pressure
R, S, T :	Viscous fluxes
t :	Physical time
u, v, w :	Cartesian velocity
W :	Conservative vectors
x, y, z :	Cartesian coordinate
x_{VG} :	Chordwise positioning of vortex generator.

Greek Symbols

α :	Angle of attack
α_{stall} :	Stall angle of attack
β :	Orientation angle of vortex generator
γ :	Specific heat ratio
ρ :	Density.

Abbreviations

DU:	Delft University
GF:	Gurney flap
NACA:	National Advisory Committee for Aeronautics
VGs:	Vortex generators
RANS:	Reynolds-averaged Navier-Stokes.

Data Availability

The data used to support the findings of this study are available from the corresponding authors upon request.

Conflicts of Interest

The authors declare that there is no conflict of interest regarding the publication of this paper.

Acknowledgments

This work was supported by the Natural Science Foundation of the Jiangsu Higher Education Institutions of China (no. 21KJB130003).

References

- [1] R. L. T. Bevan, D. J. Poole, C. B. Allen, and T. C. S. Rendall, "Adaptive surrogate-based optimization of vortex generators for tiltrotor geometry," *Journal of Aircraft*, vol. 54, no. 3, pp. 1011–1024, 2017.
- [2] D. Y. Li, H. Chang, Z. G. Zuo, H. J. Wang, and S. H. Liu, "Aerodynamic characteristics and mechanisms for bionic airfoils with different spacings," *Physics of Fluids*, vol. 33, no. 6, article 064101, 2021.
- [3] H. D. Taylor, "The elimination of diffuser separation by vortex generators," Technical Report R-4012-3, United Aircraft Corporation Connecticut, 1947.
- [4] R. Himo, C. Bou-Mosleh, and C. Habchi, "Aerodynamic performance enhancement of an airfoil using trapezoidal vortex generators," *Aircraft Engineering and Aerospace Technology*, vol. 93, no. 1, pp. 76–84, 2021.
- [5] B. B. Nia, M. Ja'fari, A. R. Ranjbar, and A. J. Jaworski, "Passive control of boundary layer flow separation on a wind turbine airfoil using vortex generators and slot," *Ocean Engineering*, vol. 283, article 115170, 2023.
- [6] P. Y. Gong, E. J. Aju, and Y. Q. Jin, "On the aerodynamic loads and flow statistics of airfoil with deformable vortex generators," *Physics of Fluids*, vol. 34, no. 6, article 067106, 2022.
- [7] D. Baldacchino, C. Ferreira, D. D. Tavernier, W. A. Timmer, and G. J. W. van Bussel, "Experimental parameter study for passive vortex generators on a 30% thick airfoil," *Wind Energy*, vol. 21, no. 9, pp. 745–765, 2018.
- [8] Z. Z. Zhao, R. F. Jiang, J. X. Feng et al., "Researches on vortex generators applied to wind turbines: a review," *Ocean Engineering*, vol. 253, article 111266, 2022.
- [9] L. Y. Gao, H. Zhang, Y. Q. Liu, and S. Han, "Effects of vortex generators on a blunt trailing-edge airfoil for wind turbines," *Renewable Energy*, vol. 76, pp. 303–311, 2015.
- [10] S. B. Verma and M. Chidambaranathan, "Swept fin-induced shock/boundary-layer separation control using corotating vortex generators," *AIAA Journal*, vol. 60, no. 11, pp. 6240–6251, 2022.
- [11] O. M. Fouatih, M. Medale, O. Imine, and B. Imine, "Design optimization of the aerodynamic passive flow control on NACA 4415 airfoil using vortex generators," *European Journal of Mechanics-B/Fluids*, vol. 56, pp. 82–96, 2016.
- [12] J. A. Weiberg and M. D. Maisel, "Wind-tunnel tests of the XV-15 tilt rotor aircraft," *NASA Technical Memorandum*, vol. 81177, 1980.
- [13] T. C. Tai, "Effect of midwing vortex generators on V-22 aircraft forward-flight aerodynamics," *Journal of Aircraft*, vol. 40, no. 4, pp. 623–630, 2003.
- [14] R. H. Liebeck, "Design of subsonic airfoils for high lift," *Journal of Aircraft*, vol. 15, no. 9, pp. 547–561, 1978.
- [15] F. Balduzzi, D. Holst, P. F. Melani et al., "Combined numerical and experimental study on the use of Gurney flaps for the performance enhancement of NACA0021 airfoil in static and dynamic conditions," *Journal of Engineering for Gas Turbines and Power*, vol. 143, no. 2, article 021004, 2021.

- [16] H. Fatahian, H. Salarian, M. E. Nimvari, and J. Khaleghinia, "Effect of Gurney flap on flow separation and aerodynamic performance of an airfoil under rain and icing conditions," *Acta Mechanica Sinica*, vol. 36, no. 3, pp. 659–677, 2020.
- [17] T. Yu, J. J. Wang, and P. F. Zhang, "Numerical simulation of Gurney flap on RAE-2822 supercritical airfoil," *Journal of Aircraft*, vol. 48, no. 5, pp. 1565–1575, 2011.
- [18] Y. Amini, H. Emdad, and M. Farid, "Adjoint shape optimization of airfoils with attached Gurney flap," *Aerospace Science and Technology*, vol. 41, pp. 216–228, 2015.
- [19] C. Dong, D. Han, and L. Yu, "Performance analysis of variable speed tail rotors with Gurney flaps," *Chinese Journal of Aeronautics*, vol. 31, no. 11, pp. 2104–2110, 2018.
- [20] V. A. Pstrikakis, R. Steijl, G. N. Barakos, and J. Małecki, "Computational aeroelastic analysis of a hovering W3 Sokol blade with Gurney flap," *Journal of Fluids and Structures*, vol. 53, pp. 96–111, 2015.
- [21] J. J. Wang, Y. C. Li, and K. S. Choi, "Gurney flap—lift enhancement, mechanisms and applications," *Progress in Aerospace Sciences*, vol. 44, no. 1, pp. 22–47, 2008.
- [22] Y. C. Li, J. J. Wang, and P. F. Zhang, "Effects of Gurney flaps on a NACA0012 airfoil," *Flow, Turbulence and Combustion*, vol. 68, no. 1, pp. 27–39, 2002.
- [23] J. C. Date and S. R. Turnock, "Computational evaluation of the periodic performance of a NACA 0012 fitted with a Gurney flap," *Journal of Fluids Engineering*, vol. 124, no. 1, pp. 227–234, 2002.
- [24] J. P. Baker, K. J. Standish, and C. P. van Dam, "Two-dimensional wind tunnel and computational investigation of a microtab modified airfoil," *Journal of Aircraft*, vol. 44, no. 2, pp. 563–572, 2007.
- [25] M. Masdari, M. Mousavi, and M. Tahani, "Dynamic stall of an airfoil with different mounting angle of Gurney flap," *Aircraft Engineering and Aerospace Technology*, vol. 92, no. 7, pp. 1037–1048, 2020.
- [26] F. F. Felker and J. S. Light, "Aerodynamic interactions between a rotor and wing in hover," *Journal of the American Helicopter Society*, vol. 33, no. 2, pp. 53–61, 1988.
- [27] C. Y. Zhu, Y. Feng, X. Shen et al., "Effects of the height and chordwise installation of the vane-type vortex generators on the unsteady aerodynamics of a wind turbine airfoil undergoing dynamic stall," *Energy*, vol. 266, article 126418, 2023.
- [28] W. Huang, Z. L. Lu, T. Q. Guo, F. Xue, and M. Zhang, "Numerical method of static aeroelastic correction and jig-shape design for large airliners," *SCIENCE CHINA Technological Sciences*, vol. 55, no. 9, pp. 2447–2452, 2012.
- [29] M. Meunier and V. Brunet, "High-lift devices performance enhancement using mechanical and air-jet vortex generators," *Journal of Aircraft*, vol. 45, no. 6, pp. 2049–2061, 2008.
- [30] M. D. Jenks and J. C. Narramore, *Final Report for the 2-D Test of Model 901 Rotor and Wing Airfoils (BSWT 592)*, Bell-Boeing Tiltrotor Team, Rept. D901-99065-1, 1984.
- [31] H. Chen and B. Chen, "Aerodynamic performance enhancement of tiltrotor aircraft wings using double-row vortex generators," *International Journal of Aeronautical and Space Sciences*, vol. 22, no. 4, pp. 802–812, 2021.
- [32] H. Chen, "Numerical investigation of the effects of vortex generators on the Bell A821201 airfoil," *Journal of the Brazilian Society of Mechanical Sciences and Engineering*, vol. 43, no. 11, p. 516, 2021.
- [33] D. Jeffrey and D. Hurst, "Aerodynamics of the Gurney flap," in *Proceedings of the 14th Applied Aerodynamics Conference*, p. 2418, New Orleans, Los Angeles, USA, 1996.